PHOTONICS Research

Wide-field *in situ* multiplexed Raman imaging with superresolution

Houkai Chen,[1] Xiaojing Wu,[2] Yuquan Zhang,[1,*] Yong Yang,[3] Changjun Min,[1] Siwei Zhu,[2] Xiaocong Yuan,[1] Qiaoliang Bao,[4] and Jing Bu[4,5]

[1]Nanophotonics Research Center, Shenzhen Key Laboratory of Micro-Scale Optical Information Technology, Shenzhen University, Shenzhen 518060, China
[2]Tianjin Union Medical Center, Tianjin 300121, China
[3]Institute of Modern Optics, Nankai University, Tianjin 300071, China
[4]College of Electronic Science and Technology, Shenzhen University, Shenzhen 518060, China
[5]e-mail: jingbu@szu.edu.cn
*Corresponding author: yqzhang@szu.edu.cn

Received 18 January 2018; revised 11 March 2018; accepted 20 March 2018; posted 23 March 2018 (Doc. ID 320120); published 30 April 2018

Because of the fingerprint-like specificity of its characteristic spectrogram, Raman spectral imaging has been applied widely in various research areas. Using a combination of structured illumination with the surface-enhanced Raman scattering (SERS) technique, wide-field Raman imaging is developed with a significant improvement in spatial resolution. As a result of the relatively narrow Raman characteristic peaks, optically encoded SERS nanoparticles can be used to perform multiplexed imaging. The results show excellent superresolution wide-field multiplexed imaging performance. The developed technique has extraordinary potential for applications in biological imaging and other related fields.

OCIS codes: (180.5655) Raman microscopy; (240.6695) Surface-enhanced Raman scattering; (100.6640) Superresolution.

https://doi.org/10.1364/PRJ.6.000530

1. INTRODUCTION

Optical microscopy plays an important role in biological research, and various microscopy approaches have been demonstrated that provide wide fields and high spatial resolution [1–5]. Fluorescent labeling methods are usually required for these methods. However, inherent inevitable shortcomings, including relatively broad emission profiles and photobleaching, are always present. In addition, biological processes commonly involve a variety of different structures and components so that a single fluorescent biomarker can hardly meet all requirements, while multiple markers usually introduce signal cross talk. The Raman spectrum, which represents the natural fingerprint of molecular structures with narrow emission profiles, provides a new approach to avoid these problems.

Various wide-field approaches for dynamic Raman imaging have been proposed over the last few decades [6–13]. Among these techniques, filter-based methods offer high compatibility with conventional optical imaging methods and low cost, although the spatial resolution of these methods is restricted by optical diffraction. Structured illumination microscopy (SIM), with its intrinsic wide-field property and high imaging speed, represents an ideal choice for wide-field and superresolution Raman imaging [3,14,15]. However, its inherent weak signal greatly restricts its practical applications. Through the use of surface-enhanced Raman scattering (SERS) techniques, exogenous SERS-type probes have provided new vision capabilities in wide-field biological imaging, biosensors, and other fields [10,16–21]. However, functionalized wide-field imaging with superresolution, especially the multiplexed ones, is rarely implemented.

In this work, we combined SIM with SERS nanoparticles to provide wide-field multiplexed imaging and achieved a high lateral resolution of 109 nm. As a benefit of the small excitation volumes of samples restricted close to the coverslip surface, the method reduces the out-of-focus signals and is highly suitable for surface imaging. The narrow emission profiles of the Raman signals are further scanned using combinable tunable filters to perform multiplexed imaging. The filter-based method is strongly compatible with conventional optical microscopy-based imaging systems. Surface biological imaging methods, and particularly time-lapse-based methods, will benefit from the technique presented here.

2. EXPERIMENTAL SETUP AND METHODS

The SIM employs spatially patterned light to illuminate a sample, to generate a moiré effect to encode undetectable high-frequency information to make such information detectable. A series of intermediate images can be captured by varying

phases of the structured patterns. Then high- and low-frequency information is separated and shifted to the corresponding positions to reconstruct superresolution images [3]. Figure 1 shows the SIM-based wide-field Raman imaging system. A 532 nm laser is used to excite the Raman signal and a spatial light modulator (SLM) (Holoeye Pluto, Germany) is used to generate two beams that are focused on the rear focal plane of an oil immersion objective lens (UApo N, 100×/1.49 oil; Olympus, Japan) and excite standing-wave evanescent structured illumination fringes on the coverslip surface. Because of the small penetration depth of evanescent waves, the illumination volume of the samples is restricted to the volume close to the surface of the coverslip. Consequently, the Raman signal excitation is confined within this small volume. The phases and directions of the illumination fringes are regulated precisely using predesigned holograms in the experiments.

A self-assembled central-wavelength tunable bandpass filter group that combines a tunable long-pass filter (TLP01-628, Semrock, U.S.) with a tunable short-pass filter (TSP01-628, Semrock, U.S.) is used to select the target Raman spectra. The orientation of the tunable filters is precisely controlled using two independent motorized rotation stages (PRM1Z8, Thorlabs, U.S.). The central wavelengths and bandwidths of the assembled bandpass filters are calibrated using a spectrometer (QE65000, Ocean Optics, U.S.). In the experiments, the full width at half-maximum (FWHM) of the bandwidth of the assembled bandpass filters is ~2 nm, which is sufficiently narrow to prevent significant spectral overlap among the targeted Raman characteristic peaks, and the transmissivity is as high as ~80%. The wide-field images are then captured using a scientific complementary metal-oxide semiconductor (sCMOS) camera (C11440-22CU, Hamamatsu, Japan) while synchronizing the camera, the SLM, and the tunable filters in the process. To increase the imaging efficiency, a flip mirror is used to switch between the wide-field imaging and spectrum measurement.

The weak inherent scattering signal is an unavoidable disadvantage in Raman imaging; however, the metal nanoparticles enhance the Raman scattering signals effectively. In this case, metal composite nanoparticles with diameters of approximately 46–50 nm composed of a gold core with a silver outer shell were used. To achieve multiplexed imaging, these SERS nanoparticles were then encoded using sorted Raman molecules: 4-mercaptophenylacetic acid (4-ATP) (Au/Ag/4-ATP, nanoparticle size of ~50 nm), 4-mercaptopyridine (4-MPY) (Au/Ag/4-MPY, nanoparticle size of ~46 nm), and 2-mercapto-4-methyl-5-thiazoleacetic acid (MMTAA) (Au/Ag/MMTAA, nanoparticle size of ~46 nm). Their Raman spectra were measured to allow the target peaks to be selected using tunable filters, as shown in Fig. 2. The discrimination of the characteristic peaks of the different Raman molecules was large enough (>2 nm) to allow these nanoparticles to be distinguished for further *in situ* multiplexed imaging.

To perform multiplexed cellular imaging, the SERS nanoparticles were conjugated with the target molecules through an EDC (1-ethyl-3-[3-dimethylaminopropyl] carbodiimide hydrochloride)-NHS (N-hydroxysuccinimide) reaction [22,23]. The nanoparticles were modified using polyallylamine (PAH) by adding 250 μL of 10 mg/mL PAH solution to a 1 mL SERS nanoparticle solution overnight at room temperature under gentle shaking conditions. After PAH modification, the nanoparticles were then conjugated with the targeted molecules [the nuclear-targeting peptide (NLS), the mitochondria-targeting peptide (MLS) and the microtube-targeting molecule alpha-Tubulin DM1A]. Small amounts of the targeted molecule solutions [NLS (100 μL, 5 μg/mL), MLS (100 μL, 5 μg/mL), and DM1A (10 μL)] were mixed with a 100 μL 10 mM EDC solution and a 20 μL 100 mM NHS solution (1 mM = 1 mmol/L). These mixtures were then incubated at room temperature for 24 h under gentle shaking conditions. Finally, the nanoparticles were centrifuged and dispersed in a culture medium solution at 4°C for experimental use.

For the intracellular Raman imaging, 3T3 cells were first cultured on coverslips for a minimum of 8 h to allow the cells to adhere to the coverslip surfaces. Then, 5 μL of the modified SERS nanoparticle solution was added to each of the culture media simultaneously, and the cells were cultured further for another 24 h to phagocytize the nanoparticles. Before the imaging experiments, the cells were washed for three times using phosphate buffer saline (PBS). Additionally, to bring more of the targeted cell structures into the illumination volume, the cells were mechanically flattened using a 1-mm-thick piece

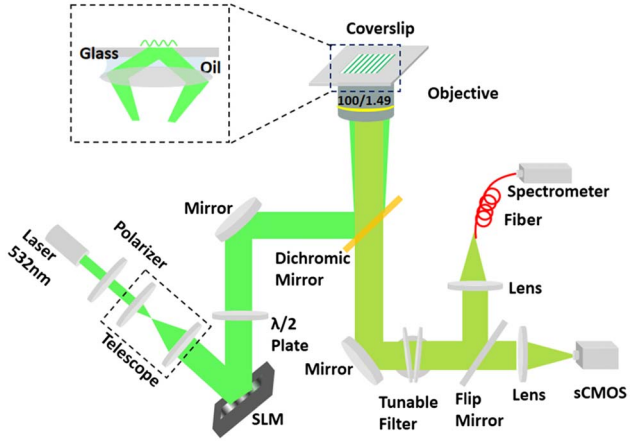

Fig. 1. Schematic of wide-field superresolution Raman imaging system.

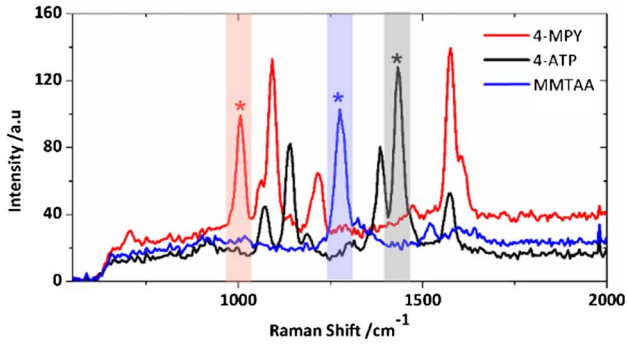

Fig. 2. Typical Raman spectra of the three different encoded SERS nanoparticles. Asterisks (*) indicate the selected peaks, and colored rectangular areas indicate the spectral regions that were used for multiplexed imaging in the experiments.

of agarose gel (~1.5 wt. %), and the agarose gel pad was then covered using a 24 mm × 24 mm coverslip [24].

3. RESULTS AND DISCUSSION

A. Stability of Raman Scattering

Photobleaching is an unavoidable problem in fluorescent imaging because of the long acquisition times or high excitation powers that are usually required. To calibrate the photostability, we measured and compared the scattering intensities of the fluorescent microspheres (diameter ~28 nm) and the SERS nanoparticles by continuous acquisition of wide-field images, as shown in Fig. 3. The Raman and fluorescent samples were deposited separately on coverslip surfaces and measured under the same conditions with a laser power of 15 mW. Compared with conventional fluorescence signals, the SERS nanoparticles showed much greater stability. From these results, it was found that the fluorescent scattering signal was quickly bleached to less than 5% of the initial scattering intensity, and most of the fluorescence thus vanished, as shown by the results in Figs. 3(a) and 3(b). For the red curve shown in Fig. 3(a), though photobleaching of the Raman scattering was also observed, the final intensity stabilized at a level of no less than 20% of the initial intensity. In the experiments, smaller laser powers (11 mW) could obviously reduce the attenuation of the Raman scattering; the final Raman scattering intensity then stabilized at more than 45% of the initial intensity and remained stable until the end of the measurement process. To keep the stability of signals, all measurements were implemented several minutes after illumination.

B. Wide-Field Multiplexed Imaging of SERS Nanoparticles

The lateral resolution is of vital importance for wide-field multiplexed imaging systems. Therefore, for evaluation, three spectrally distinct SERS nanoparticles were initially mixed and imaged. The mixed solution of Raman molecule-encoded SERS nanoparticles was deposited on a coverslip surface and dried in the atmosphere. During the experiments, the nanoparticles were immersed in water to mimic an intracellular fluid environment. The structured illumination was implemented in two perpendicular directions, and six intermediate images were captured for each superresolution image reconstruction. This capture process was repeated for every bandpass filter. Figure 4(a) shows a conventional wide-field image of the SERS nanoparticles, and Fig. 4(b) is the reconstructed superresolution image. The three primary colors, i.e., red, green, and blue, are used to represent the three different SERS nanoparticles. By measuring the FWHM values of the Gaussian fittings of the normalized intensity profiles of the framed nanoparticles shown in Figs. 4(a) and 4(b), the lateral resolution was suppressed from 269 to 109 nm, representing an improvement of more than twice that of conventional wide-field imaging, as shown in Fig. 4(c).

In these images, the primary colors are not very pure for two main reasons. First, aggregation of different SERS nanoparticles is uncontrollable, and the separation distance may be smaller than the resolution of the system, so it is difficult to distinguish the overlap among different adjacent nanoparticles. Second, Raman signals of different molecules in the junction regions between adjacent nanoparticles are simultaneously enhanced

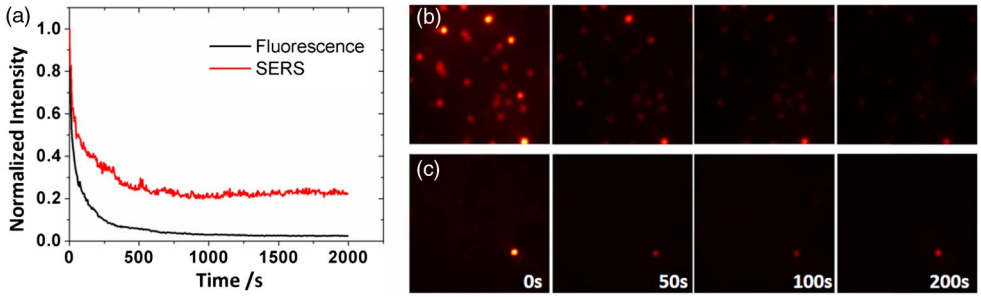

Fig. 3. (a) Normalized intensities of fluorescent scattering and Raman scattering signals over time. The signals were detected at a frame rate of 0.2 Hz over an exposure time of 0.3 s. The red curve represents the Raman signal, and the black curve represents the fluorescent signal. (b) and (c) show time-lapse images of the fluorescent microspheres and the SERS nanoparticles, respectively.

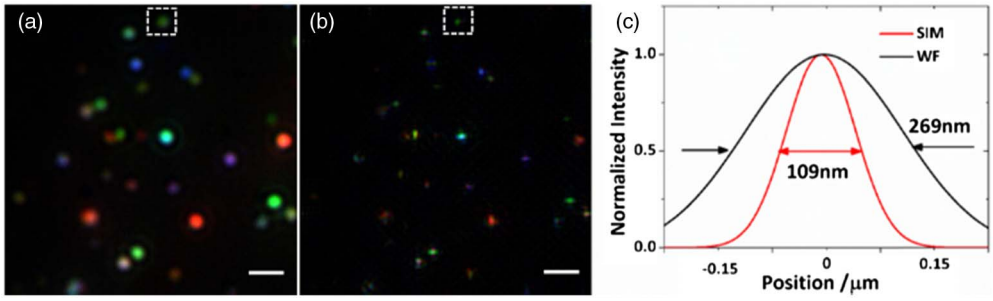

Fig. 4. Wide-field imaging of the SERS nanoparticles. (a) Conventional imaging results and (b) the reconstructed wide-field image; (c) Gaussian fitting profiles of the normalized intensity of the images framed in (a) and (b). Scale bar: 1 μm.

to be detected; this is known as the dimer enhancement [25]. However, efficiency of the dimer enhancement is closely related to the polarization direction of the illumination light. Consequently, the isotropy of the spatial resolution of these reconstructed wide-field images can be seriously affected by variable polarization directions [10]. Therefore, the polarization direction is kept unchanged at an angle of 45° with respect to the horizontal directions during the experiments, and its enhancement effects on the different directions of illumination are essentially suppressed in this work.

C. Multiplexed Imaging of 3T3 Cells

On this basis, we further implemented such a conceptual multiplexed imaging technique for use in biological applications. Three organelles of 3T3 cells were labeled using surface-modified Raman molecule-encoded nanotags: the Au/Ag/4-MPY SERS nanoparticles labeled nucleus were imaged in the red layer, the Au/Ag/4-ATP SERS nanoparticles labeled microtubes were imaged in green, and the Au/Ag/MMTAA SERS nanoparticles labeled mitochondria were imaged in blue. Figure 5(a) shows the bright field image of the 3T3 cells before Raman imaging; Figs. 5(b) and 5(c) show the enlarged overlaid wide-field images of the area in dashed frame shown in Fig. 5(a), before and after reconstruction, respectively. The results clearly show that more details were resolved after reconstruction. Because of the small penetration depth of the evanescent waves, the detected signals were confined within a small volume close to the coverslip surface, and this explains why only a few signals were detected during the experiments. Furthermore, this small penetration depth helped to improve signal-to-noise ratio (SNR) in surface imaging.

These results confirm that the wide-field Raman imaging method has a multiplexed imaging capability and that higher multiplexed images are feasible by adding appropriate Raman reporter molecules. However, the reconstructions in the cells still show imperfections when compared with those of the SERS nanoparticles shown in Fig. 4. The main reason for these imperfections is that the complex intracellular environment seriously affects the quality of both intermediate images and reconstruction. Stable bonding of the SERS probes in the intracellular environment will require further consideration in future work. High SNR is also an important factor; thus SERS nanoparticles with higher enhancement and photostability would be very beneficial, and further optimization of the SERS nanoparticles will provide more effective results.

D. Discussion

In the wide-field Raman experiments, SERS signals are all excited simultaneously using the same laser, avoiding the need for different sources and thus helping to simplify the illumination system and reduce the system cost to a large extent. For most imaging techniques, the resolution (both spectral and spatial resolutions) always conflict with imaging time, and a balance between resolution and imaging speed is necessary. The proposed method is thus a great candidate method for such cases. It can essentially provide the high imaging speeds of the wide-field method and a relatively high spatial resolution beyond the diffraction limit simultaneously. The spectral resolution of ~2 nm is enough to distinguish various SERS nanoprobes for multiplexed imaging and can be further improved. For the proposed method, exposure time for an intermediate image is 10 s, and the reconstruction process is no more than 1 s. Therefore, actually, the main factor restricting the imaging speed is the camera sensitivity in this work. With help of more sensitive cameras, such as the electron multiplying charge-coupled device (EMCCD) camera, the imaging speed will be significantly improved.

4. CONCLUSIONS

In summary, we have demonstrated a new concept for a wide-field multiplexed imaging technique that combines SIM and optically encoded SERS nanoparticle labeling. The method provides high spatial resolution that is far beyond the diffraction limit in a wide field. Wide-field multiplexed imaging could also be achieved through simultaneous using of multiple labels. With functionalized SERS nanoparticles, multiple specific structures in cells can be labeled and imaged simultaneously. Though the method is still in its preliminary stage of development, it shows powerful potential in biological applications, particularly for time-lapse imaging of living samples. It is expected to be beneficial for research in biology, medicine, and other related fields.

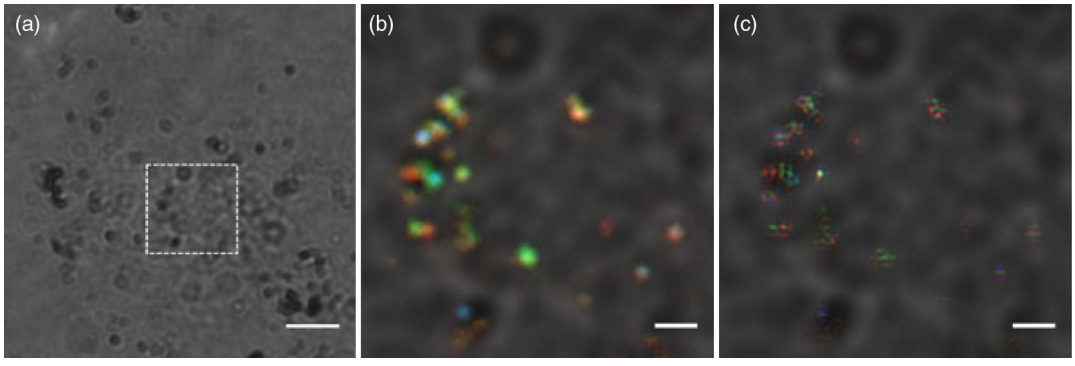

Fig. 5. Multiplexed imaging of 3T3 cells labeled using surface-modified SERS nanoparticles. (a) Bright field image of 3T3 cell, and (b) conventional and (c) reconstructed wide-field pseudo-color images overlaid with the framed bright field image from (a). Scale bars: 5 μm in (a), and 1 μm in (b) and (c).

Funding. National Natural Science Foundation of China (NSFC) (61490712, 61427819, 91750205, 61605117); National Key Basic Research Program of China (973) (2015CB352004); Leading Talents of Guangdong Province Program (00201505); Natural Science Foundation of Guangdong Province (2016A030312010, 2016A030310063, 2017A030313351); National Key Research and Development Program of China (2016YFC0102401); Science and Technology Innovation Commission of Shenzhen (KQTD2017033011044403, KQTD20150710165601O1, ZDSYS201703031605029); Excellent Young Teacher Program of Guangdong Province (YQ2014151).

Acknowledgment. The authors gratefully thank Prof. Zhuyuan Wang and Shenfei Zong for providing the SERS nanoparticles.

REFERENCES

1. S. W. Hell and J. Wichmann, "Breaking the diffraction resolution limit by stimulated emission: stimulated-emission-depletion fluorescence microscopy," Opt. Lett. **19**, 780–782 (1994).
2. M. J. Rust, M. Bates, and X. Zhuang, "Sub-diffraction-limit imaging by stochastic optical reconstruction microscopy (STORM)," Nat. Methods **3**, 793–796 (2006).
3. M. G. Gustafsson, "Surpassing the lateral resolution limit by a factor of two using structured illumination microscopy," J. Microsc. **198**, 82–87 (2000).
4. E. Betzig, G. H. Patterson, R. Sougrat, O. W. Lindwasser, S. Olenych, J. S. Bonifacino, M. W. Davidson, J. Lippincott-Schwartz, and H. F. Hess, "Imaging intracellular fluorescent proteins at nanometer resolution," Science **313**, 1642–1645 (2006).
5. F. Chen, P. W. Tillberg, and E. S. Boyden, "Expansion microscopy," Science **347**, 543–548 (2015).
6. R. J. Mallia, P. Z. McVeigh, C. J. Fisher, I. Veilleux, and B. C. Wilson, "Wide-field multiplexed imaging of EGFR-targeted cancers using topical application of NIR SERS nanoprobes," Nanomedicine **10**, 89–101 (2015).
7. S. Yang, B. Li, A. Akkus, O. Akkus, and L. Lang, "Wide-field Raman imaging of dental lesions," Analyst **139**, 3107–3114 (2014).
8. P. Z. McVeigh, R. J. Mallia, I. Veilleux, and B. C. Wilson, "Widefield quantitative multiplex surface enhanced Raman scattering imaging in vivo," J. Biomed. Opt. **18**, 046011 (2013).
9. R. J. Mallia, P. Z. McVeigh, I. Veilleux, and B. C. Wilson, "Filter-based method for background removal in high-sensitivity wide-field-surface-enhanced Raman scattering imaging in vivo," J. Biomed. Opt. **17**, 076017 (2012).
10. S. Hennig, V. Mönkemöller, C. Böger, M. Müller, and T. Huser, "Nanoparticles as nonfluorescent analogues of fluorophores for optical nanoscopy," ACS Nano **9**, 6196–6205 (2015).
11. J. Ma and D. Ben-Amotz, "Rapid micro-Raman imaging using fiber-bundle image compression," Appl. Spectrosc. **51**, 1845–1848 (1997).
12. H. R. Morris, C. C. Hoyt, P. Miller, and P. J. Treado, "Liquid crystal tunable filter Raman chemical imaging," Appl. Spectrosc. **50**, 805–811 (1996).
13. P. J. Treado, I. W. Levin, and E. N. Lewis, "High-fidelity Raman imaging spectrometry: a rapid method using an acousto-optic tunable filter," Appl. Spectrosc. **46**, 1211–1216 (1992).
14. Y. Hirano, A. Matsuda, and Y. Hiraoka, "Recent advancements in structured-illumination microscopy toward live-cell imaging," Microscopy **64**, 237–249 (2015).
15. Q. Li, M. Reinig, D. Kamiyama, B. Huang, X. Tao, A. Bardales, and J. Kubby, "Woofer-tweeter adaptive optical structured illumination microscopy," Photon. Res. **5**, 329–334 (2017).
16. Z. Wang, S. Zong, L. Wu, D. Zhu, and Y. Cui, "SERS-activated platforms for immunoassay: probes, encoding methods, and applications," Chem. Rev. **117**, 7910–7963 (2017).
17. Y. Liu, H. Zhou, Z. Hu, G. Yu, D. Yang, and J. Zhao, "Label and label-free based surface-enhanced Raman scattering for pathogen bacteria detection: a review," Biosens. Bioelectron. **94**, 131–140 (2017).
18. P. L. Stiles, J. A. Dieringer, N. C. Shah, and R. P. Van Duyne, "Surface-enhanced Raman spectroscopy," Annu. Rev. Anal. Chem. **1**, 601–626 (2008).
19. A. F. Palonpon, J. Ando, H. Yamakoshi, K. Dodo, M. Sodeoka, S. Kawata, and K. Fujita, "Raman and SERS microscopy for molecular imaging of live cells," Nat. Protoc. **8**, 677–692 (2013).
20. H. Xu, C. Kan, C. Miao, C. Wang, J. Wei, Y. Ni, B. Lu, and D. Shi, "Synthesis of high-purity silver nanorods with tunable plasmonic properties and sensor behavior," Photon. Res. **5**, 27–32 (2017).
21. H. Chen, S. Wang, Y. Zhang, Y. Yang, H. Fang, S. Zhu, and X. Yuan, "Structured illumination for wide-field Raman imaging of cell membranes," Opt. Commun. **402**, 221–225 (2017).
22. Y. Chen, J.-Q. Ren, X.-G. Zhang, D.-Y. Wu, A.-G. Shen, and J.-M. Hu, "Alkyne-modulated surface-enhanced Raman scattering-palette for optical interference-free and multiplex cellular imaging," Anal. Chem. **88**, 6115–6119 (2016).
23. Y. Chen, X. Bai, L. Su, Z. Du, A. Shen, A. Materny, and J. Hu, "Combined labelled and label-free SERS probes for triplex three-dimensional cellular imaging," Sci. Rep. **6**, 19173 (2016).
24. P. Kner, B. B. Chhun, E. R. Griffis, L. Winoto, and M. G. Gustafsson, "Super-resolution video microscopy of live cells by structured illumination," Nat. Methods **6**, 339–342 (2009).
25. K. D. Alexander, K. Skinner, S. Zhang, H. Wei, and R. Lopez, "Tunable SERS in gold nanorod dimers through strain control on an elastomeric substrate," Nano Lett. **10**, 4488–4493 (2010).